First-order versus second-order phase transformation in AuZn

M. Sanati,[1,2,*] R. C. Albers,[2] T. Lookman,[2] and A. Saxena[2]
[1]*Physics Department, Texas Tech University, Lubbock, Texas 79409-1051, USA*
[2]*Theoretical Division, Los Alamos National Laboratory, Los Alamos, New Mexico 89404, USA*
(Received 29 January 2013; published 16 July 2013)

The first-order versus second-order nature of the phase transition in AuZn has been examined by first-principles calculations. The calculated elastic constants of the high-temperature $B2$ phase have a large anisotropy, which suggests a possible instability in this phase. The first-principles calculations were extended to finite temperature by including vibrational and electronic contributions to the free energy. A small free-energy barrier was found between the high- ($B2$) and low-temperature (R) phases, which indicates that this is a weak first-order phase transition. Finally, we find that the calculated theoretical transformation temperature and entropy change (small latent heat) are in excellent agreement with the experimental observations for a first-order transition. Based on the entropy calculations for both phases, the high-temperature phase is found to be stabilized by the contribution of low-energy phonon modes to the lattice entropy.

DOI: 10.1103/PhysRevB.88.024110 PACS number(s): 31.15.A−, 81.30.−t, 63.70.+h

I. INTRODUCTION

Around a concentration of 50%, the phase diagrams of the β-brass alloys A_xB_{1-x}, where A is one of the Cu, Ag, or Au noble metals and B is one of the divalent Zn or Cd metals, have bcc-like β phases at high temperatures. In most of these alloys, the β phase is site-disordered at high temperatures, then orders into a CsCl-type (or $B2$) crystal structure as the temperature is lowered, and finally undergoes a martensitic transformation at even lower temperatures.[1] In the special case of the AuZn alloys, the site disorder seems to be absent and the ordered CsCl crystal structure exists even up to the melting temperature.[2]

What makes AuZn alloys more unusual in this class of alloys, however, is that Lashley *et al.*[3] have claimed to have observed a continuous second-order phase transition at exactly the stoichiometric $x = 50\%$ concentration rather than the martensitic phase transformation seen off stoichiometry (where x is either greater than or less than 50%). In this paper, we attempt to understand and make sense of this and earlier work for stoichiometric AuZn,[1,3–9] in which this solid-solid phase transformation was studied from the high-temperature (austenite-like) CsCl phase structure to the low-temperature (martensite-like) rhombohedral (R-phase) structure.[10] It is interesting to note that the complexity of this phase transition has even led Darling *et al.*[8] to conjecture that this point in the phase diagram might be a "critical point" joining two first-order curves (that occur away from stoichiometry) when the phase diagram is plotted as a function of temperature and concentration. While this might not be the precisely correct technical description of this type of point in a phase diagram, it does suggest how special the 50% concentration is compared to other concentrations that appear to clearly have first-order transitions. Why the 50% concentration AuZn material is so special relative to other concentrations and related materials is not completely clear at this point in time. We can only conjecture that it might be related to the strong ordering tendency observed in AuZn, possibly caused by the large atomic-size mismatch between the Au and Zn atoms.

If the 50%-concentration transition is indeed second order, this makes stoichiometric AuZn of even greater interest, since the vast majority of all phase transformations in solid materials are first-order phase transformations.[11] In contrast to the previous experimental work on AuZn that has proposed that the low-temperature phase transformation is continuous, in this paper we instead examine the question from a theoretical point of view. As will be explained below, our calculations indicate that the stoichiometric 50%-concentration material actually exhibits a first-order phase transition, albeit with a very weak free-energy barrier that masks this first-order character and hence explains the experimental tendencies toward second-order behavior. Our result is also consistent with the first-order nature of the phase transformations away from the 50% perfect stoichiometry. Based on our calculations, we consider that all concentrations of the AuZn alloy have first-order transformations. The only difference for the stoichiometric 50%-concentration material is that the transformation has a smaller free-energy barrier than other concentrations.

To understand the dilemmas posed by the current experimental evidence in AuZn materials,[3,7–9] it is useful to briefly review the main differences in experimentally observed physical properties between first- and second-order phase transformations, which in this section we will abbreviate by FOP and SOP, respectively, since we use this terminology so heavily here. The traditional nomenclature for the order of a phase transition was made by Ehrenfest, who labeled these by the lowest derivative of the free energy that is discontinuous at the transition temperature. Thus, FOPs have a discontinuity in the first derivative of the free energy, and SOPs have a discontinuity in the second derivative. In practice, for a solid, this means that the volume and entropy are discontinuous in a FOP and continuous in a SOP. This implies a latent heat for the transition in a FOP and no latent heat in a SOP. In addition, for FOPs, the specific heat is always finite at the transition temperature, whereas it goes to infinity for SOPs (this is often called a λ-like behavior with reference to the prototype for this behavior in liquid helium). There is an experimental controversy in AuZn about whether a λ-like behavior has actually been observed for this material.

Most solid-solid phase transformations are first-order transitions that involve diffusion of the atoms from one crystal structure to another. Martensitic phase transformations are a

special subclass of first-order transitions that differ from the general case in that they are diffusionless and displacive. The diffusionless nature of the transition means that the atoms move continuously from one crystal structure to the next during the transition by coordinated "military" motions that are small compared to nearest-neighbor distances. Hence, one can define a microscopic path between the low- and high-temperature phases that typically involves the coordinated positions of many atoms in a supercell of the high-temperature phase. Theoretically, this path is determined by minimizing the free energy as the system continuously distorts from one phase into the other. In the literature,[12–15] there have been numerous calculations of such martensitic paths, and we will provide an example of this below for AuZn. In terms of transformation kinetics, the atomic motions of these paths proceed near the speed of sound in martensitic transformations and are usually too fast to be experimentally observed. It appears as if the lattice instantaneously changes from one crystal structure to another when the material transforms.

Martensitic transitions are also displacive, which means that the lattice is continuously deformed relative to the overall shape of the crystal and usually with a change in crystal symmetry. For example, a cubic lattice could continuously distort into a tetragonal lattice by lengthening one direction of the cube. The displacive nature of the transformation leads to orientation relationships between the austenite and martensite and consequently habit planes and other phenomenologies in the metallurgical descriptions of these types of phase transformations. The microscopic pathway of the transition must, of course, include these shape deformations in a continuous way.

For the rest of this paper, we specialize our discussion to phase transitions that are both diffusionless and displacive, since this is what is relevant to AuZn and its alloys. If the transition can be characterized as first-order in the Ehrenfest thermodynamic sense, it is martensitic. If it is continuous, we will call it martensitic-like. In addition, for the rest of the paper we will use the typical language of martensites for both types of transformation, calling the high-temperature phase austenite and the low-temperature phase martensite, and the phase transformation temperature T_M.

Within the context of martensitic and martensitic-like transformations, the distinction between a first-order and second-order phase transition can be reframed as asking whether or not the continuous path of the atoms from the austenite to the martensite has a free-energy barrier at the phase-transformation temperature T_M. If the free-energy barrier exists, then the phase transformation will necessarily be a martensitic first-order transition, and will involve a discontinuous change of crystal structure at T_M. If the free-energy barrier does not exist, the phase transformation will be a second-order transition and the equilibrium crystal structure will continuously distort from the high-temperature crystal structure to the fully developed low-temperature crystal structure in a gradual manner as the temperature is lowered (perhaps over a small temperature range). In addition, if the transformation is continuous, then there cannot be a simultaneous coexistence of both phases, which is a standard phenomenological experimental indication for a martensitic transformation.

The presence or absence of this free-energy barrier also has important consequences for many of the other properties of the phase transition. For example, having such a barrier often leads to hysteresis at the transition temperature, since the barrier forces nucleation behavior in order to convert one phase to the other, and, in the absence of some kind of dirt or defect that can serve as a nucleation center, it can lead to undercooling or overheating to drive the conversion, since thermal fluctuations may not be big enough to provide a driving force to overcome the energy barrier. Another consequence, which is an important signature of an FOP, is the simultaneous coexistence of both phases (a "mixed-phase region"). In contrast, a SOP can immediately convert since no free-energy barrier needs to be overcome in order to cause the conversion, and hence nucleation phenomena need not be considered. For similar reasons, SOPs usually have divergent susceptibilities and long-range power-law decays of correlations, where the correlation length goes to infinity at the transition. Most of this behavior is studied in the subject area of "critical phenomena," involving universality classes and critical exponents.

Another issue that is related to the energy barrier that frequently arises in FOP/SOP discussions for these classes of materials is that of phonon softening at the phase transition. If a phonon mode goes to zero at the phase-transition temperature, this implies that the crystal structure can continuously distort without cost in free energy from the high-temperature parent (higher symmetry) crystal phase to the "frozen phonon" crystal structure of the low-temperature phase. Hence, there would be no barrier to the phase transition and the transition might be a SOP. The other possibility is an incomplete phonon softening, where the phonon heads toward zero but never quite makes it at the transition point, as might occur in AuZn. Krumhansl and Gooding[19] have shown that such a case can be a weak FOP instead of a SOP.

From a theoretical point of view that is based on first-principles electronic-structure calculations, such as we use, it is much easier to distinguish between a FOP and a SOP by calculating the free-energy barrier rather than relying on the traditional continuity or discontinuity of derivatives of the free energy. In this paper, we will show theoretically that AuZn has a weak first-order phase transition. By "weak" we mean that the energy of the transition temperature, $k_B T$, or the relevant thermal fluctuation energy, is larger than the free-energy barrier between the two phases. Weak first-order phase transitions can have very small latent heats, pseudocritical phenomena, and other properties very similar to second-order phase transitions. Essentially, the free-energy barrier between the two phases is so small compared to the thermal fluctuations that it can seem almost as if there is no energy barrier present, and hence the material can appear to be very second-order-like in its properties.

Therefore, the difference between a weak FOP and a SOP could be extremely difficult to distinguish experimentally. For example, a very weak FOP would have very large but finite correlation lengths. If large enough, this might seem similar to the infinite correlation lengths present in SOPs. This complex situation is confused further if the material is not perfectly pure and if defects may be present. Many papers have shown (see, e.g., Refs. 16, 17, and 18) that a weak first-order transition can sometimes mask a second-order phase transition, since it is

TABLE I. Calculated lattice constants (a and c), elastic constants (C_{ij}), shear anisotropy (A, dimensionless), and bulk modulus B at zero temperature and the comparison of these quantities with available experimental data.

Phase	a (Å)	c (Å)	θ (deg)	C_{44} (GPa)	C' (GPa)	A	B (GPa)
$B2$	3.195		90	62.00	6.00	10.38	114.3
expt. ($B2$)	3.126,[a] 3.149[b,c]		90	66.60,[b] 62.26[c]	6.66,[b] 6.72[c]	10,[b] 9.26[c]	122.0,[b] 138.4[c]
R	7.816	5.545	89.99				120.0
expt. (R)	7.658[a]	5.476[a]	89.55[a]				

[a]Reference 5.
[b]Reference 8.
[c]Reference 35.

possible to convert a true second-order transition to a first-order transition by the application of external fields, which could also possibly include dirt or defect structures in the material. These considerations explain the current ongoing controversy over AuZn, where the true nature of the phase transition has been strongly debated.

So far there has been no systematic theoretical study on austenite and martensite phases of AuZn, and the number of experimental studies are also limited. Hence, important information, such as crystal lattice structure and phonon densities of states, is lacking. In the present investigation, we use first-principles methods to study the formation of the $B2$ and R phases in AuZn system. This paper is organized as follow: Section II discusses the details of the calculations. Section III contains the results for crystal parameters, elastic properties, and phonon dispersion along the [110] direction of austenite ($B2$) phase. Section IV deals with the thermal properties and stability of the $B2$ and R phases at zero and finite temperatures. A summary of our findings and a conclusion are presented in Sec. V.

II. METHODOLOGY

Our electronic-structure calculations have been carried out using the first-principles density-functional pseudopotential packages VASP[20–22] and SIESTA[23,24] within the generalized-gradient approximation (GGA) to the exchange-correlation potential as parametrized by Perdew-Burke-Ernzerhof (Ref. 25). In most of our calculations we have used VASP, since SIESTA was only used to analyze the bonding (Mulliken populations analysis) between the atoms.

In the VASP code, we used the projector augmented-wave method[26,27] with a cutoff kinetic energy of 346 eV. Electronic degrees of freedom were optimized with a conjugate-gradient algorithm, and both external and internal cell parameters are fully relaxed. The crystal was represented by an 18-atom periodic cell. A modified tetrahedron method[28] ($6 \times 6 \times 7$ mesh) was used for the k-point integration in the Brillouin zone.

The dynamical matrix calculations were performed using a force-constant method with 36-atom, 54-atom (for $B2$ phonon dispersion calculations), and 72-atom unit cells with a k-point sampling[29] of $4 \times 4 \times 2$, $8 \times 8 \times 8$, and $4 \times 2 \times 2$, respectively. We used an atomic displacement of 0.0211 Å for the entire phonon calculations presented in this work. The dynamical matrices were obtained from the Fourier transform of the real-space force-constant matrices. The eigenfrequencies and eigenvectors were obtained from a diagonalization of the dynamical matrix. All of the force constants were calculated for the lattice constant with the minimum total energy (i.e., the lattice constants for each different method that are given in Table I).

The SIESTA calculations used norm-conserving pseudopotentials in the Troullier-Martins form[30] to remove the core regions from the calculations. The basis sets for the valence states are linear combinations of numerical atomic orbitals.[23,31,32] In the present calculations, we used double-zeta polarized basis sets (two sets of valence s's and p's plus one set of d's). The charge density is projected on a real-space grid with an equivalent cutoff of 150 Ry to calculate the exchange-correlation and Hartree potentials.

III. HIGH-TEMPERATURE-PHASE CRYSTAL STRUCTURE AND ELASTIC PROPERTIES

The austenite (or high-temperature) phase of AuZn is an ordered body-centered-cubic (bcc-like CsCl-type or $B2$) structure. The equilibrium volume (lattice constant) was obtained by fitting the total energy-volume data with Murnaghan's equation of state.[33] The equilibrium lattice constants from the zero-temperature VASP and SIESTA calculations are in very good agreement with experiment, with VASP predicting a slightly larger value (3.195 Å) while SIESTA predicts a smaller value (3.059 Å). The difference is related to the different pseudopotentials used, since the exchange-correlation potential used was the same in both calculations.

Depending on the symmetry of the crystal structure, calculations of the elastic constants require using different distortions of the crystal structure. A lattice with cubic symmetry has three independent elastic constants: C_{11}, C_{12}, and C_{44}. For the AuZn $B2$ structure, the elastic constant C_{44} was obtained from the monoclinic volume-conserving distortion,[34]

$$\epsilon = \begin{pmatrix} 0 & \delta/2 & 0 \\ \delta/2 & 0 & 0 \\ 0 & 0 & \delta^2/(4-\delta^2) \end{pmatrix},$$

where the energy increase (per unit cell volume) is given by

$$E(\delta) = \tfrac{1}{2} C_{44} \delta^2 + O(\delta^4). \quad (1)$$

Similarly, the shear modulus C' [$C' = \frac{1}{2}(C_{11} - C_{12})$] is obtained from the tetragonal volume-conserving distortion,[34]

$$\epsilon = \begin{pmatrix} \delta & 0 & 0 \\ 0 & -\delta & 0 \\ 0 & 0 & \delta^2/(1-\delta^2) \end{pmatrix}.$$

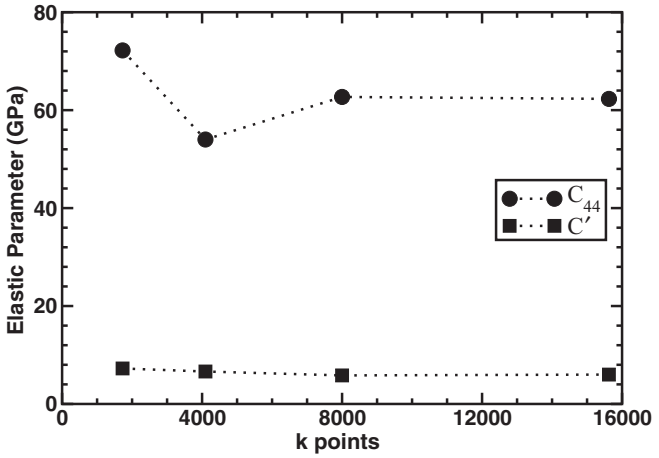

FIG. 1. Calculated C_{44} and C' elastic parameters as a function of k points.

The relation between the energy increase (per unit cell volume) and the distortion δ is given by

$$E(\delta) = 2C'\delta^2 + O(\delta^4). \quad (2)$$

The bulk modulus for a cubic crystal is equal to $B = (C_{11} + 2C_{12})/3$ and can be obtained from the second derivative of the energy-volume curve. C_{11} and C_{12} can be obtained from the calculated bulk modulus and C'. To ensure the convergence of the elastic parameters with respect to the k-point sampling, we have used $12 \times 12 \times 12$, $16 \times 16 \times 16$, $20 \times 20 \times 20$, and $25 \times 25 \times 25$ meshes. As is shown in Fig. 1, the elastic parameters are converged for the $20 \times 20 \times 20$ (8000 point) mesh.

Calculated elastic constants (for the $25 \times 25 \times 25$ mesh) and the Zener anisotropy factor A (the ratio of C_{44} to C') are given in Table I, and they are in excellent agreement with experimental measurements.[3,35] According to Zener,[36] the large value of A is an indication of a structural instability of the system and hence a tendency for a phase transformation. The AuZn system has a very low shear modulus (Fig. 1). The origin of the small shear modulus can be understood in terms of bonding between the atoms. A Mulliken population analysis gives a weak metallic bonding between the Au and Zn atoms. Furthermore, it indicates that there are antibonding states for d_{z^2} and $d_{x^2-y^2}$ orbitals of a Zn atom. A study of the charge density (Fig. 2) shows that electrostatic interactions are partially shielded by valence charges along the [001] directions. This effect, in addition to the lack of any bonding along the high-symmetry [001] directions, is why there is such a small resistance to a shear distortion.

It should be noted that all of these first-principles electronic-structure calculations are, of course, like all such calculations, done at zero temperature, whereas the experimental data are at finite temperature. However, the thermal corrections are expected to be small for these properties. Later sections of the paper will add finite-temperature corrections for other properties.

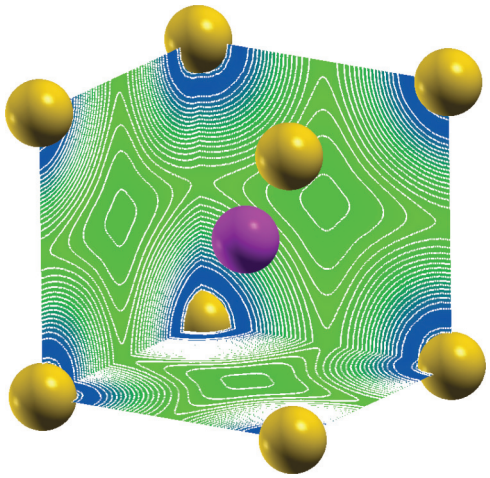

FIG. 2. (Color online) Calculated charge density of AuZn for cuts in [100], [010], and [001] planes.

IV. $B2$- TO R-PHASE TRANSFORMATION

A. Phase-transformation path at $T = 0$ K

Theoretical methods at finite temperature need to include the effects of thermal vibrations, which are difficult to accurately calculate. In contrast, there exist many first-principles local-density approximation codes that can fairly precisely calculate total-energy differences at zero temperature between different crystal structures, and which also include algorithms for determining the optimized structure for any constraint placed on the system and hence along any given path. For this reason, it is valuable to consider the minimum-energy atomic pathway between the two phases at zero temperature and the relevant energy barrier along this path.

In AuZn, there is strong evidence that the austenite and martensite crystal structures are related by a "frozen phonon" in the high-temperature phase. As we will show later, this is not exactly accurate, since additional atomic distortions within a larger unit cell of the low-temperature phase must also be allowed to relax to exactly describe the low-temperature crystal structure. Nonetheless, it is relevant to examine the phonon spectra of the high-temperature crystal structure. This can be calculated at zero temperature by electronic-structure methods described above. For a continuous phase transformation, it is often expected that this "frozen-phonon" mode will have a significant temperature dependence, having a finite frequency at high temperatures and then gradually softening all the way to zero frequency at the phase-transition temperature. If this is the case, our zero-temperature phonon mode should then have an imaginary frequency (indicating an unstable crystal structure with respect to the low-temperature phase). On the other hand, if our zero-temperature phonon has a finite frequency, then it is highly likely that there is no instability of this phonon mode at higher temperatures, since our phonon calculations are for the crystal structure that is stable at high temperatures.

The experimental phonon dispersion curves of the $B2$ phase along the [110] direction show a continuous softening of the TA_2 phonons as the temperature is reduced from high temperatures, confirming the instability of the high-temperature austenite phase. Calculated and measured TA_2 phonon dispersion curves along [110] are shown in Fig. 3. All

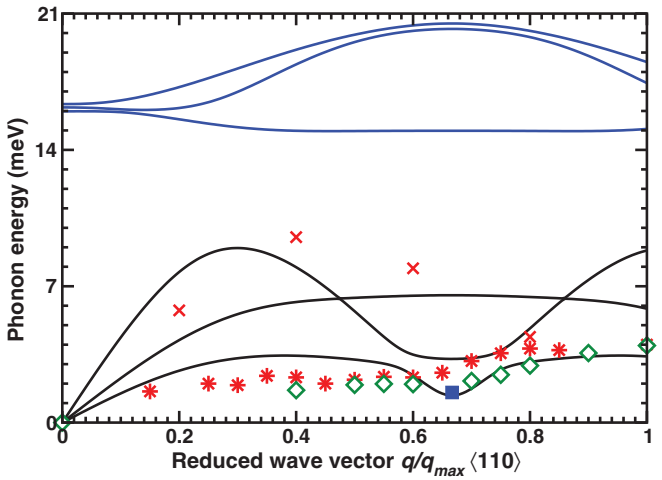

FIG. 3. (Color online) Calculated (solid lines) and experimental phonon dispersion relations of the [110] branch. The red stars (*) and crosses (×) are data of Ref. 6 for [110] phonons. The star is the TA_2 mode (taken from Fig. 1 of the reference for an alloy with a concentration of 51.5 at. % of Zn and a temperature of 110 K) and the cross is the LA mode (taken from Fig. 3 of the reference for an alloy with a concentration of 48.5 at. % of Zn and at room temperature). The green diamonds are the stoichiometric TA_2 phonon data of Ref. 3 at 200 K. The blue square represents the phonon frequency (energy) obtained from our frozen phonon calculation.

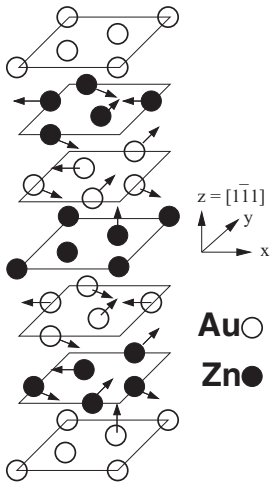

FIG. 4. The crystal structure of the martensite R phase. Arrows indicate the directions of atomic displacements from the ideal $B2$ position.

of our phonon calculations for $B2$ structure are done at the theoretical minimum lattice constant (3.195 Å). The phonons along TA_2 direction are very sensitive to lattice constant values. For example a choice of slightly large lattice constant (3.20 Å) could produce imaginary phonons, instead of the positive low frequency value we find for the soft phonon. Note that all phonon calculations in this paper are for a 72-atom unit cell, unless otherwise specified. For the experimental data at low temperatures, it is difficult to find good phonon dispersion curves. The TA_2[110] phonon mode has been measured by Lashley *et al.*[3] at 200 and 300 K. For other phonons and other temperatures, we have had to refer to Makita *et al.*,[6] which unfortunately only presents data at slightly off stoichiometry, at 48.5 and 51.5 at. % Zn.

Our theoretical results predict an incomplete softening of the phonons at $q/q_{\max} = (\frac{2}{3},\frac{2}{3},0)$ at zero temperature, which is more pronounced than the higher-temperature experimental measurements. Since we expect the zero-temperature results to have the maximum instability toward the low-temperature martensitic phase, our phonon calculations strongly suggest that there is likely to be no soft mode or "frozen phonon" at any temperature in AuZn in the austenite phase. The lowest temperature for which the experimental phonon spectra have been measured is 110 K, and the temperature dependence of the spectra does not show any signs of softening to zero frequency at any lower temperature, which is consistent with our calculations.

The phonon calculations require a description of the crystal structures. The martensite phase is a rhombohedral structure (R phase). The conventional rhombohedral unit cell is formed by 27 unit cells of the $B2$ austenite phase. However, this can be reduced into a primitive hexagonal unit cell containing nine $B2$ cells. The high-temperature $B2$ phase and its relation with the R phase is shown in Fig. 4. The unit-cell vectors $\vec{a}_1$, $\vec{a}_2$, and $\vec{a}_3$ are along the [121], [1$\bar{1}\bar{2}$], and [$\bar{1}$1$\bar{1}$] directions of the cubic $B2$ unit cell, respectively. The details of the crystal structure and atomic positions are given in Ref. 5. The R phase is a distorted $B2$ structure with P3 symmetry that has 18 atoms per unit cell. We have calculated the theoretical structure by minimizing the total energy of the electronic structure as a function of the internal atomic coordinates. The internal positions of the atoms are given in Table II. The interplanar distances between neighboring planes in the R phase (Fig. 4) are not equal. The distance between the first-second, second-third, third-fourth, fourth-fifth, fifth-sixth, and sixth-seventh are 0.2, 0.2, 0.1, 0.2, 0.2, and 0.1 (in units of c/a), respectively. This can be understood in terms of size mismatch between Au and Zn atoms. The Au atom in the first plane and the Zn atom in the fourth plane (Fig. 4) are displaced out of the planes significantly (about 0.13 c/a unit), causing the nonuniform distribution of planes. The transformation from the $B2$ to the R phase and the crystal structure of the R phase are very similar to that for the AuCd martensitic transformation.[38]

The phase transformation is a combination of external (shear) and internal (shuffle) distortions, i.e., a shear of the overall unit cell and internal atomic relaxations. It is not

TABLE II. Refined atomic positions for the R phase with P3 symmetry (International Table[37] space-group number 143).

Site	x	y	z
Au(1a)	0	0	0
Au(1b)	1/3	2/3	0.12957
Au(1c)	2/3	1/3	0
Au(3d)	0.33347	−0.01541	0.41295
Au(3d)	0.69291	0.01895	0.70528
Zn(1a)	0	0	0.5
Zn(1b)	1/3	2/3	0.63221
Zn(1c)	2/3	1/3	0.5
Zn(3d)	0.33332	−0.01881	0.91195
Zn(3d)	0.68291	0.01625	0.20599

clear which one occurs first or if both occur simultaneously. Because of the complicated displacements of the atoms and the number of parameters involved in this process, the mechanism (path) of the phase transformation in the AuZn system is not yet completely understood.

However, the low-energy phonon of the TA_2 branch at $q/q_{\max} = (\frac{2}{3},\frac{2}{3},0)$ suggests the possible path and displacement of atoms for this transformation. The displacement of atoms along the z axis ($[1\bar{1}1]$ of the $B2$ unit cell) corresponds to a phonon with a wave vector of $q/q_{\max} = (\frac{2}{3},\frac{2}{3},0)$ and transverse polarization (TA_2). By a small perturbation of atoms along that direction, our calculations show that the Au atom in the first plane and the Zn atom in the fourth plane (Fig. 4) are displaced by similar amplitudes, while the rest of the atoms remain very close to their equilibrium positions. Using a frozen-phonon approach, and by displacing only those two atoms, we can calculate the phonon frequency (energy) for such a mode.

The calculated energy of the frozen phonon is in excellent agreement with our results obtained from the direct method (Fig. 3). Therefore, we expect that AuZn has the lowest energy barrier in that direction. However, the displacement of only those two atoms involved in the frozen phonon is less than the number of available internal distortions of the atoms, while still maintaining the R-phase symmetry, and additional atomic relaxations must therefore be considered. In our calculations, this is determined by allowing the other atoms to distort in any way that is allowed by crystal symmetry that will lower the total energy.

Figure 5 shows the different energy versus displacement calculations for frozen-phonon and relaxed calculations. The path that was followed in this figure was calculated by moving the Zn atom in the fourth plane [Zn(1b)] and then allowing other relaxations of the other atoms as described below in the 18-atom unit cell. The value for $u_{\max}$ was determined from the fully relaxed R phase that we have just described above. Calculations of martensitic pathways for other materials[12–15] have often used the more sophisticated and computationally efficient nudged-elastic band method.[39] The results should be the same in either case, as long as the lowest-energy path is found.

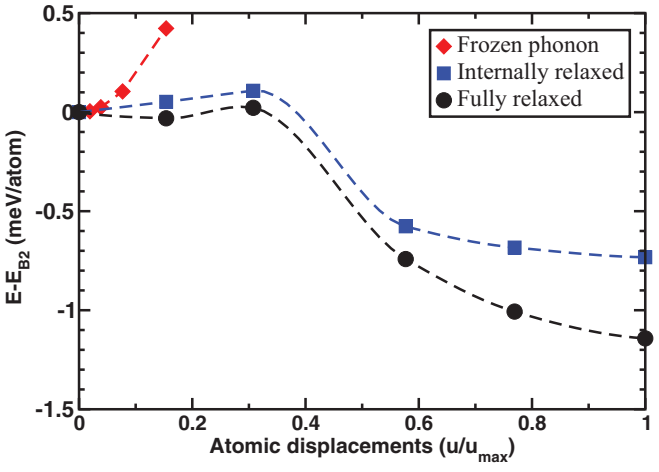

FIG. 5. (Color online) The energy difference at zero temperature for a path involving the displacement of atoms from the $B2$ position toward the R-phase atomic coordinates (see text for a more complete description of how the path was determined). E_{B2} is the ground-state energy of the $B2$ structure and $u_{\max}$ is the maximum atomic displacement (the difference between atomic position in the R and $B2$ phases) for the Zn atom in the fourth plane.

In the frozen-phonon calculations, only the two atoms of Au and Zn in the first and fourth planes have been displaced with a similar amplitude [Au(1b) and Zn(1b)]. Further investigations confirmed that the small displacement of the Zn atom in the fourth plane along $[1\bar{1}1]$ of the $B2$ unit cell caused the Au atom in the first plane to also displace in a similar direction and with a similar amplitude (and vice versa), while the other atoms remained close to their ideal $B2$ coordinates. Therefore, in the next set of calculations, which are described in the figure as "internally relaxed," only the Zn atom in the fourth plane was displaced and the positions (internal coordinates) of the other 17 atoms were optimized by minimizing the total energy. Finally, in the last set of calculations ("fully relaxed"), both the internal atomic coordinates and the lattice constants (a, c, and θ, cf. Table I) were relaxed. Note that for small-displacement values, all of the energy calculations are very similar to each other, i.e., the displacement of the Au atom in the first plane and the Zn atom in the fourth plane along $[1\bar{1}1]$ of the $B2$ unit cell is the start of the phase transformation. Further movement of those atoms requires the internal relaxation of atoms.

In Fig. 5 it is important to note for both the internally and fully relaxed calculations that the energy barriers have similar heights. Hence, the atoms can internally relax into the R-phase atomic positions, and then the external relaxation can occur or both the internal and external relaxation can happen at the same time. In either case, the atomic shuffles (changing the internal positions of the atoms within the unit cell) are the dominant effect in the $B2$ to R phase transformation, and the effective Landau free energy for this system can be parametrized in terms of a shuffle parameter as the primary order parameter.[40,41]

B. Phase transformation at finite temperature

In a second-order phase transformation, the order parameter changes continuously between the two phases, in contrast to the first-order one where it changes discontinuously, like a step function.[42] This steplike behavior is typical of reconstructive transitions (with no group-subgroup relation between the phases) between fully ordered phases. In the Landau model for second-order phase transformations, at and below the transition temperature, one should see a continuous change of order parameter without any region of stability for both phases (i.e., it is not possible for the austenite and martensite to simultaneously coexist), requiring the complete softening of the associated phonon.[19] Our phonon calculations (at $T = 0$ K) along the [110] direction (Fig. 3) showed a softening (but not a complete one). This result is also indirectly verified by the positive curvature of energy versus the atomic displacement plot (Fig. 5), confirming the stability of the $B2$ phase even at $T = 0$ K. However, the most important result is the existence of a small barrier between the $B2$ and R phases (Fig. 5). This barrier separates the $B2$ and R phases at zero temperature, causing a region of coexistence for both phases, opposite to what should happen in a second-order phase transformation. Since the predicted height of the barrier is very small (about

2 K), it is unlikely to be able to be detected experimentally, and, at the transformation temperature, the $B2$ structure should easily be able to transform into the R phase through normal thermal fluctuations.

Ideally, in order to theoretically determine whether the phase transformation is first or second order, the free-energy path should be calculated at the transition temperature to examine whether a free-energy barrier exists (first-order transition) or not (second-order transition). To do this, both external and internal distortions of the unit cell and atomic positions should be allowed to relax along the path. Since each point (including all the possible relaxations) would require a separate phonon calculation to determine the free energy (i.e., to include the thermal vibrations), this would require a large number of expensive calculations well beyond our current computer resources. It is therefore important instead to make some approximations to estimate whether the free-energy barrier is likely to exist or not. We have already tested one limiting case, that of zero temperature (see above). If there were no energy barrier for this case (the most unstable case), it would strongly indicate that the phase transformation at the transition temperature also would have no energy barrier. However, since we did find a small energy barrier for this case, our starting position has to therefore be that of assuming a first-order transition. Nonetheless, because the zero-temperature barrier is so small, it is always possible that even for a transition temperature as low as 64.5 K, the thermal entropy could reduce or eliminate the free-energy barrier.

Since it is too computationally expensive to calculate the full path, we have made the approximation that the lowest free-energy path at the transition temperature is similar to that at zero temperature. Thus, we have calculated the free energy at the transition temperature for the path that has the same identical lattice constants and internal atomic coordinates that were found for the fully relaxed zero-temperature path (cf. Fig. 5). Since the transformation temperature is very low (64.5 K), we have used the Helmholtz free energy (constant volume) instead of the Gibbs free energy. The vibrational modes of the crystal are usually a much more important contribution to the free energy of the system than the electronic contribution. At high temperatures, near the melting point, it is very important to include anharmonic effects on the phonon spectra. However, in cases like AuZn where the phase-transition temperature is low, the vibrational free energy F_{vib} can be accurately calculated within the harmonic approximation.[43] This is given by

$$F_{\text{vib}}(T) = 3k_B T \int_{\Omega} \ln\left\{2\sinh\left(\frac{\hbar\omega}{2k_B T}\right)\right\} g(\omega)d\omega. \qquad (3)$$

It would be useful to compare our total phonon density of states (PDOS) $g(\omega)$ with experiment. Unfortunately, there are no experimental measurements of the optical phonons for AuZn systems, and even the acoustic phonons are measured only along a few high-symmetry directions and for a limited number of modes. Therefore, it is impossible to extract any total PDOS from experimental measurements. Nonetheless, based on the excellent agreement between experimental measurement of the acoustic phonons of the $B2$ phase and the calculated phonons in high-symmetry directions as depicted in Figs. 3 and 6, we believe that the total PDOS presented here is likely to be very accurate. In Fig. 7, the results for the total PDOS for the $B2$ and R phases at $T = 0$ K for 36- and 72-atom cells are shown. The calculated phonon density of states consists of two sets of bands separated by a gap for both structures. The Au-related modes are at low energies and those of Zn are at higher energies (frequencies). In the $B2$ structure, the phonons in both bands are narrower than the R phase. Increasing the size of the unit cell improved the optical modes, while there was no significant change for acoustic modes. Since the acoustic phonons contribute more to the vibrational free energy (entropy) than the optical ones do, as is shown later in the paper, the free-energy calculations with the 72-atom unit cell are not much improved relative to the 36-atom cell.

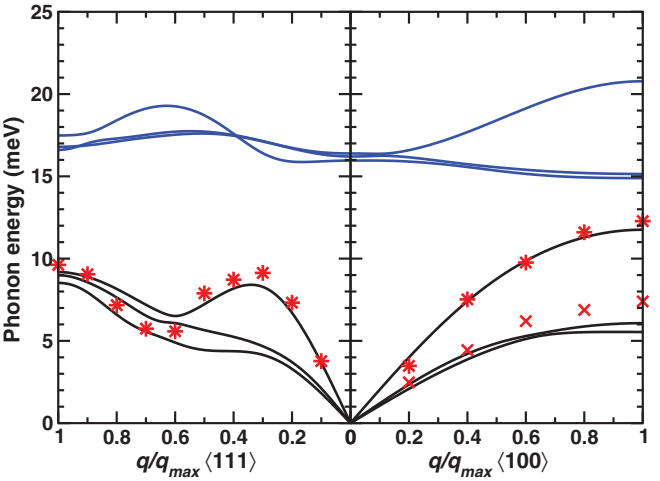

FIG. 6. (Color online) The phonon dispersion curves of the AuZn $B2$ phase. All the phonon experimental data shown (stars and crosses) are taken from Ref. 6 at room temperature. The stars on the left side of the figure are for the [111] LA phonon mode (from Fig. 2 of the reference at a 51.5 atomic percentage of Zn). The stars and crosses on the right side of the figure are the LA and TA_2 [100] phonon modes (from Fig. 3 of the reference at a 48.5 atomic percentage of Zn).

Another contribution to the total free energy of solids comes from their electronic entropy. In this case, the electronic

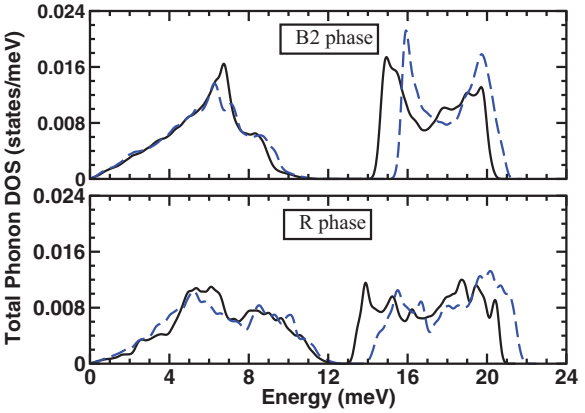

FIG. 7. (Color online) Total PDOS of $B2$ (top) and R (bottom) phases calculated with 36- (blue dashed line) and 72- (black solid line) atom cells.

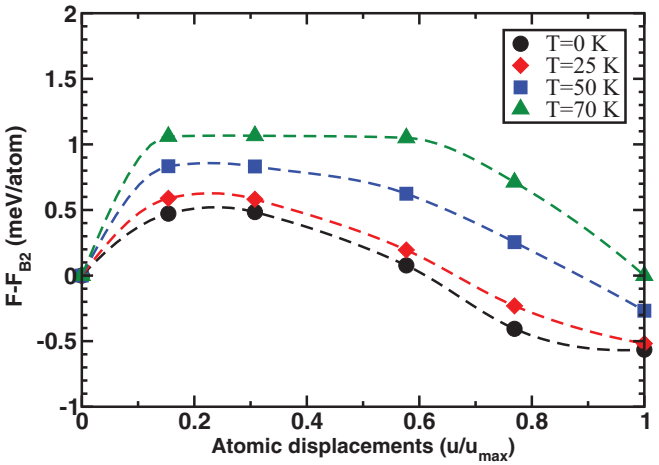

FIG. 8. (Color online) The Helmholtz free energy of the R phase and the atomic displaced structures with respect to the $B2$ phase as a function of temperature. The calculated transformation temperatures are 70 and 65 K for 36- and 72-atom cells, respectively (cf. Fig. 9).

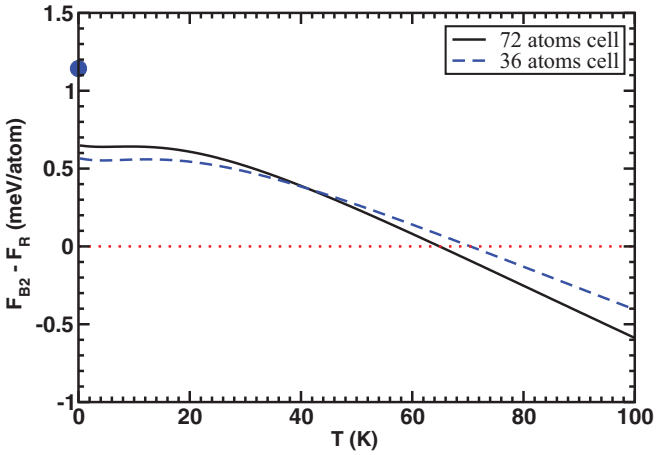

FIG. 9. (Color online) The total Helmholtz free-energy difference between $B2$ and R phases as a function of temperature for 36- and 72-atom unit cells. The calculated transformation temperature for the 72-atom cell is at 68.5 K. The R phase is stable below this temperature, while the $B2$ phase is more stable above it. The difference in electronic energy between these two structures is shown by a solid circle.

contribution to the free energy depends on the electronic density of states as a function of volume, $n(E)$. The occupation of these states, given by the Fermi distribution

$$f(E,T) = [e^{(E-E_f)/(K_B T)} + 1]^{-1}, \quad (4)$$

determines their entropy,[44,45]

$$S_{\rm el}(T) = -k_B \int [f \ln f + (1-f)\ln(1-f)] n(E) dE, \quad (5)$$

and hence the electronic contribution to the free energy, $F_E(T,V) = -T S_{\rm el}(T,V)$. Although the electronic entropy terms are not large, we have included them in our calculations for completeness.

The free-energy path as a function of temperature is depicted in Fig. 8 (see the description above for how the path was determined). We find that including the vibrational contribution to the free energy increases the barrier height as a function of temperature from the $T = 0$ K value of 0.3 meV/atom, and hence the effect of temperature actually tends to stabilize the first-order transformation relative to a second-order continuous transition. In these calculations, we used a 36-atom cell for calculating the phonons and the Helmholtz free energy. As can be seen from Fig. 9, the transition temperature obtained from the 36-atom cell phonon calculations is comparable to that of the 72-atom cell, and is in excellent agreement with what was measured experimentally. The zero-temperature free energy in this figure differs from that of the energy shown in Fig. 5 by the addition of the zero-point energy contribution along the path. The calculated barrier at temperatures close to the transition temperature is about 1 meV/atom (11.5 K). Although it is possible that other atomic distortions of the crystal structure could still lower or remove this free-energy barrier, it would seem unlikely. Hence, we believe that stoichiometric AuZn is indeed a weakly first-order phase transformation at the transition temperature (i.e., a finite free-energy barrier exists at this temperature).

Finally, we have calculated the first-order AuZn phase-transformation temperature and entropy to see how well they compare with experiment. The vibrational entropy and specific heat at constant volume were calculated by using the first and second derivatives of the Helmholtz free energy.[43]

Figure 9 shows the difference between the Helmholtz free energies of the $B2$ and R structures. The phonon DOSs are calculated for 36- and 72-atom cells in order to consider the finite-size effects on the transition temperature. Above 65 and 70 K, the $B2$ structure is more stable than the R phase for 36- and 72-atom cells, respectively. By reducing the temperature below these temperatures, the R phase forms. This result is in excellent agreement with the observed temperature of 64.5 K.[3,8] The slight difference can be caused by underestimating the phonon frequency of the $B2$ phase along the [011] direction (Fig. 3). The shift of acoustic phonons in the $B2$ phase to lower frequencies with respect to the R structure (Fig. 7) causes a higher vibrational entropy that stabilizes the austenite phase at high temperatures. By lowering the temperature, the vibrational entropy contribution yields the vibrational and electronic energies, and the $B2$ structure transforms to the lower-symmetry R phase. This is in complete agreement with Zener's studies on bcc materials with low shear (low vibrational frequency) resistance.[36]

Calculated specific heat at constant volume as a function of temperature and its comparison with experimental measurement are depicted in Fig. 10. However, the most interesting finding is the discontinuity of vibrational entropy at the transformation temperature (Fig. 11). The calculated entropy change is 2.79 J/mol K for the 72-atom unit-cell phonon calculations. Darling *et al.*[8] experimentally estimated the entropy change by integration of C/T from $T_1 = 47.5$ K to $T_2 = 67.0$ K and found a value of 2.02 J/mol K. This is in very good agreement with our calculated value, and the slight difference can be related to the nature of calculations. We have also determined the entropy for the

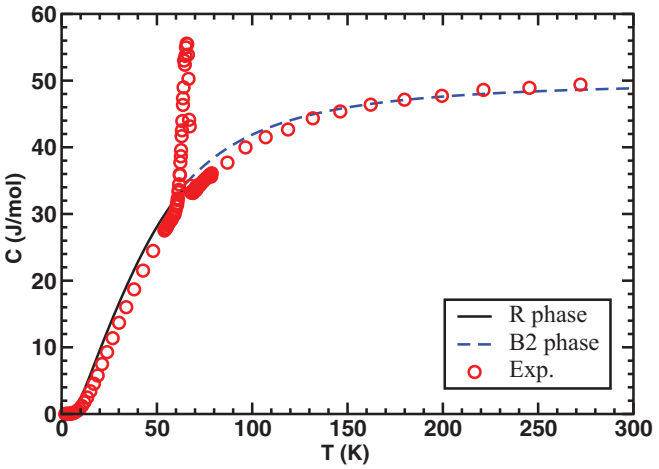

FIG. 10. (Color online) Calculated heat capacity of $B2$ (dashed line) and R (solid line) phases as a function of temperature. Experimental data (taken from Ref. 8) are shown by solid circles.

less accurate 36-atom unit-cell phonon calculations, and we obtained a value of 2.46 J/mol K. The difference between the smaller and larger unit-cell calculations is about 10%, which suggests that our results are converged at least to this level in unit-cell size.

In a temperature-induced second-order phase transformation, the presence of an external field breaks the symmetry and can transform it into a first-order transition. However, the effect of the external field on a weakly first-order transformation has different consequences. In this case, the applied field could shift the transformation temperature instead of suppressing the transformation.[18] Also, under certain conditions it can transform a weakly discontinuous transformation into a continuous one. According to our first-principles calculations for AuZn, the latent heat and the energy barrier for this martensitic transformation are very small. Therefore, any external and/or internal strain, such as pressure, impurities, or vacancies, could have a significant impact and lead to a wrong conclusion about the true nature of phase transformation in the AuZn system. Hence, our conclusion that AuZn is a weakly first-order phase transition is for the pure material in the absence of defects. If defects are present, the situation might be unclear. In any case, it is probably difficult to experimentally determine the difference between such a weakly first-order transition and a true second-order transition.

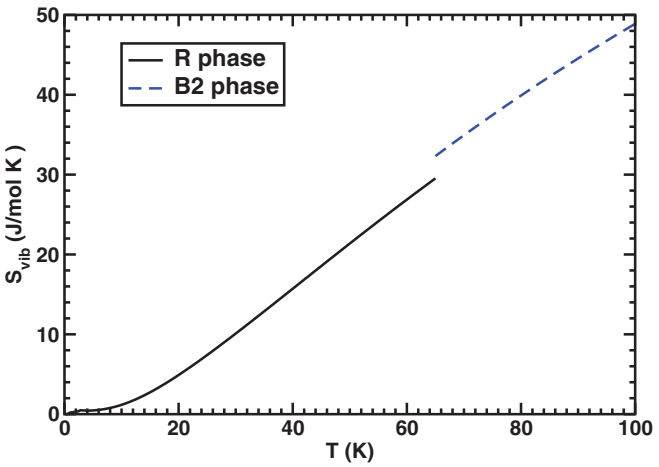

FIG. 11. (Color online) Calculated vibrational entropy of $B2$ and R phases as a function of temperature. At transformation temperature there is a small discontinuity in entropies (latent heat).

V. SUMMARY

We have shown that the phase transition in AuZn is a weak first-order transition with a small free-energy barrier between the phases at the transition temperature that is much smaller than the available thermal fluctuation energy. For this reason, the phenomenology of the transition in many ways exhibits properties associated more with a second-order phase transition rather than a first-order transition. This result is satisfying in that it no longer makes the 50% concentration so special (for no apparent reason). With our result, we have now shown that the AuZn system has a first-order transition at all concentrations. The only difference for the 50% concentration is that the free-energy barrier is smaller than for other concentrations. We can speculate that this is due to the strong site-ordering tendency for stoichiometric AuZn due to the large mismatch in the atomic sizes of the Au and Zn atoms, but we have not demonstrated this.

In addition, we have performed first-principles calculations for both the high- and low-temperature phases of stoichiometric AuZn. The lattice and elastic parameters were calculated and compared with the available experimental data. The phonon dispersion curves along high-symmetry directions for the $B2$ phase were also calculated. We found that the acoustic branches are in good agreement with experimental measurements. In addition, the phonon density of states for both the austenite (high-temperature) and martensite (low-temperature) phases was theoretically determined.

It was shown that there is no complete softening of the phonons for the $B2$ austenite phase as required by the Landau model of second-order phase transitions. Also at zero temperature, our first-principles calculations confirm the existence of an energy barrier between the two phases, creating a region of stability and coexistence for both of the phases. Estimates of the changes in free energy at the transition temperature strongly suggest that the free-energy barrier continues to exist also at the phase-transition temperature.

Finally, we have calculated the relevant contributions to the free energy of the austenite and martensite phases, with the vibrational free energy obtained from first-principles calculations of the phonon spectra in the harmonic approximation, and the electronic entropy free-energy contribution from first-principles electronic-structure calculations. The resulting phase-transition temperature and change in entropy were found to be in excellent agreement with the experimental measurements.

ACKNOWLEDGMENTS

This work was carried out under the auspices of the National Nuclear Security Administration of the U.S. Department of Energy at Los Alamos National Laboratory under Contract No. DE-AC52-06NA25396. We also acknowledge the generous amount of computer time provided by Texas Tech University High Performance Computer Center.

*m.sanati@ttu.edu

[1] H. Pops and T. B. Massalski, Trans. Met. Soc. AIME **233**, 728 (1965).

[2] Reference 1 presents phase diagrams around the 50% alloy concentrations for Cu-Zn, Ag-Zn, and Au-Zn, including the low-temperature regime needed to show the martensites. It also presents more detailed information about this class of alloys that we have summarized in this first paragraph.

[3] J. C. Lashley, S. M. Shapiro, B. L. Winn, C. P. Opeil, M. E. Manley, A. Alatas, W. Ratcliff, T. Park, R. A. Fisher, B. Mihaila, P. Riseborough, E. K. H. Salje, and J. L. Smith, Phys. Rev. Lett. **101**, 135703 (2008).

[4] H. Okamoto and T. B. Massalski, Bull. Alloy Phase Diag. **10**, 59 (1989).

[5] K. Krompholz and A. Weiss, Ber. Bunsenges. Phys. Chem. **82**, 334 (1978).

[6] T. Makita, A. Nagasawa, Y. Morii, N. Minakawa, and H. Ohno, Physica B **213-214**, 430 (1995).

[7] B. Winn, S. M. Shaprio, J. C. Lashley, C. Opeil, and W. Ratcliff, J. Phys. C **251**, 012027 (2010).

[8] T. W. Darling, F. Chu, A. Migliori, D. J. Thoma, M. Lopez, J. C. Lashley, B. E. Lang, J. Boerio-Goates, and B. F. Woodfield, Philos. Mag. B **82**, 825 (2002).

[9] J. C. Lashley, B. E. Lang, J. Boerio-Goates, and B. F. Woodfield, J. Chem. Therm. **34**, 251 (2002).

[10] The trigonal crystal structure was identified by Makita *et al.*, Ref. 6, from x-ray powder-diffraction data. They also related this martensitic crystal structure to that seen for AuCd alloys.

[11] H. B. Callen, *Thermodynamics and an Introduction to Thermostatics*, 2nd ed. (Wiley, New York, 1985).

[12] D. R. Trinkle, R. G. Hennig, S. G. Srinivasan, D. M. Hatch, M. D. Jones, H. T. Stokes, R. C. Albers, and J. W. Wilkins, Phys. Rev. Lett. **91**, 025701 (2003).

[13] D. R. Trinkle, D. M. Hatch, H. T. Stokes, R. G. Hennig, and R. C. Albers, Phys. Rev. B **72**, 014105 (2005).

[14] R. G. Hennig, D. R. Trinkle, J. Bouchet, S. G. Srinivasan, R. C. Albers, and J. W. Wilkins, Nat. Mater. **4**, 129 (2005).

[15] A. Lew, K. Caspersen, E. Carter, and M. Ortiz, J. Mech. Phys. Solids **54**, 1276 (2006).

[16] A. I. Larkin and S. A. Pikin, Zh. Eksp. Teor. Fiz. **56**, 1664 (1969) [Sov. Phys. JETP **29**, 891 (1969)].

[17] G. A. Baker and J. W. Essam, Phys. Rev. Lett. **24**, 447 (1970).

[18] M. A. Fradkin, Pis'ma Zh. Eksp. Teor. Fiz. **63**, 594 (1996) [JETP Lett. **63**, 628 (1996)]; Phys. Rev. B **50**, 16326 (1994).

[19] J. A. Krumhansl and R. J. Gooding, Phys. Rev. B **39**, 3047 (1989).

[20] VASP 2003 at http://cms.mpi.univie.ac.at/vasp.

[21] G. Kresse and J. Hafner, Phys. Rev. B **47**, 558 (1993).

[22] G. Kresse and J. Furthmüller, Phys. Rev. B **54**, 11169 (1996).

[23] D. Sanchez-Portal, P. Ordejón, E. Artacho, and J. M. Soler, Int. J. Quantum Chem. **65**, 453 (1997).

[24] E. Artacho, D. Sánchez-Portal, P. Ordejón, A. García, and J. M. Soler, Phys. Status Solidi B **215**, 809 (1999).

[25] J. P. Perdew, K. Burke, and M. Ernzerhof, Phys. Rev. Lett. **77**, 3865 (1996).

[26] P. E. Blöchl, Phys. Rev. B **50**, 17953 (1994).

[27] G. Kresse and D. Joubert, Phys. Rev. B **59**, 1758 (1999).

[28] P. E. Blöchl, O. Jepsen, and O. K. Andersen, Phys. Rev. B **49**, 16223 (1994).

[29] H. J. Monkhorst and J. D. Pack, Phys. Rev. B **13**, 5188 (1976).

[30] N. Troullier and J. L. Martins, Phys. Rev. B **43**, 1993 (1991).

[31] O. F. Sankey and D. J. Niklewski, Phys. Rev. B **40**, 3979 (1989); O. F. Sankey, D. J. Niklewski, D. A. Drabold, and J. D. Dow, *ibid.* **41**, 12750 (1990).

[32] A. A. Demkov, J. Ortega, O. F. Sankey, and M. P. Grumbach, Phys. Rev. B **52**, 1618 (1995).

[33] F. D. Murnaghan, Proc. Natl. Acad. Sci. (U.S.A.) **30**, 244 (1944).

[34] M. J. Mehl, J. E. Osburn, D. A. Papaconstantopoulos, and B. M. Klein, Phys. Rev. B **41**, 10311 (1990).

[35] R. J. Schiltz, T. S. Prevender, and J. F. Smith, J. Appl. Phys. **42**, 4680 (1971).

[36] C. Zener, Phys. Rev. **71**, 846 (1947).

[37] *International Tables for Crystallography, Volume A, Space Group Symmetry*, 5th ed., edited by Th. Hahn (Kluwer Academic, Dordrecht, 2002).

[38] T. Ohba, Y. Emura, and K. Otsuka, Mater. Trans. JIM **33**, 29 (1992).

[39] H. Jónsson, G. Mills, and K. W. Jacobsen, in *Classical and Quantum Dynamics in Condensed Phase Simulations*, edited by B. J. Berne, G. Ciccotti, and D. F. Coker (World Scientific, Singapore, 1998), p. 385.

[40] G. R. Barsch, Mater. Sci. Forum **327-328**, 367 (2000).

[41] M. Sanati, A. Saxena, T. Lookman, and R. C. Albers, Phys. Rev. B **63**, 224114 (2001).

[42] P. Tolédano, G. Krexner, M. Prem, H.-P. Weber, and V. P. Dmitriev, Phys. Rev. B **64**, 144104 (2001).

[43] A. A. Maradudin, E. W. Montroll, G. H. Weiss, and I. P. Ipatova, *Theory of Lattice Dynamics in the Harmonic Approximation* (Academic, New York, 1971).

[44] R. E. Watson and M. Weinert, in *Solid State Physics*, edited by H. Ehrenreich and F. Spaepen (Academic, San Diego, 2001), Vol. 56, p. 85.

[45] M. Sanati, R. C. Albers, T. Lookman, and A. Saxena, J. Phys.: Condens. Matter **23**, 295501 (2011).